PHYSICAL REVIEW D **91,** 054002 (2015)

Strategies for probing nonminimal dark sectors at colliders: The interplay between cuts and kinematic distributions

Keith R. Dienes,[1,2,*] Shufang Su,[1,†] and Brooks Thomas[3,‡]

[1]*Department of Physics, University of Arizona, Tucson, Arizona 85721 USA*
[2]*Department of Physics, University of Maryland, College Park, Maryland 20742 USA*
[3]*Department of Physics, Carleton University, Ottawa, Ontario K1S 5B6 Canada*

(Received 17 July 2014; published 3 March 2015)

In this paper, we examine the strategies and prospects for distinguishing between traditional dark-matter models and models with nonminimal dark sectors—including models of Dynamical Dark Matter—at hadron colliders. For concreteness, we focus on events with two hadronic jets and large missing transverse energy at the Large Hadron Collider (LHC). As we discuss, simple "bump-hunting" searches are not sufficient; probing nonminimal dark sectors typically requires an analysis of the actual shapes of the distributions of relevant kinematic variables. We therefore begin by identifying those kinematic variables whose distributions are particularly suited to this task. However, as we demonstrate, this then leads to a number of additional subtleties, since cuts imposed on the data for the purpose of background reduction can at the same time have the unintended consequence of distorting these distributions in unexpected ways, thereby obscuring signals of new physics. We therefore proceed to study the *correlations* between several of the most popular relevant kinematic variables currently on the market, and investigate how imposing cuts on one or more of these variables can impact the distributions of others. Finally, we combine our results in order to assess the prospects for distinguishing nonminimal dark sectors in this channel at the upgraded LHC.

DOI: 10.1103/PhysRevD.91.054002 PACS numbers: 95.35.+d, 13.85.−t, 14.80.−j

I. INTRODUCTION

Overwhelming evidence now suggests [1] that nonbaryonic dark matter contributes a substantial fraction $\Omega_{\rm CDM} \approx 0.26$ [2] of the energy density in the Universe. Experimental and observational data significantly constrain the fundamental properties of the particle(s) which contribute toward this dark-matter abundance. Nevertheless, a broad range of viable theoretical possibilities exists for what the dark matter in our Universe might be. One possibility is that the dark sector is "minimal" in the sense that a single, stable particle species contributes essentially the entirety of $\Omega_{\rm CDM}$. However, there also exist additional well-motivated possibilities in which the dark sector manifests a richer and more complicated *nonminimal* structure. For example, several particle species could contribute nontrivially toward $\Omega_{\rm CDM}$ [3–5]. Indeed, $\Omega_{\rm CDM}$ could even represent the collective contribution from a vast ensemble of potentially unstable individual particle species whose lifetimes are balanced against their cosmological abundances—a possibility known as Dynamical Dark Matter (DDM) [5]. Other extensions of the minimal case exist as well. Thus, once an unambiguous signal of dark matter is identified, differentiating between all of these possibilities will become the next crucial task for dark-matter phenomenology.

This task presents a unique set of challenges. Practically by definition, the dark sector comprises neutral particle species with similar or identical quantum numbers under the Standard-Model (SM) gauge group. Indeed, many theoretical realizations of the dark sector differ from one another only in the multiplicity and/or masses of such particle species and the strengths of their couplings to other fields in the theory. For this reason, evidence for a particular structure within the dark sector is not usually expected to manifest itself via the simultaneous observation of signal excesses in multiple detection channels. Rather, such evidence will often appear only in the shapes of the distributions of particular kinematic quantities in one particular channel. Such distributions include, for example, the recoil-energy spectra obtained from direct-detection experiments, the energy spectra of photons or other cosmic-ray particles at indirect-detection experiments, and the distributions of a number of kinematic variables (particle momenta, invariant and transverse masses, etc.) at colliders. Of course, some information about the properties of the dark particles can be ascertained merely by identifying the kinematic endpoints of these distributions. However, such information is typically insufficient to distinguish single-particle from multiparticle dark sectors. Indeed, for such purposes, an analysis of the full *shape* of the distribution is required.

In many experimental contexts, the extraction of information from kinematic distributions is complicated by the presence of sizeable backgrounds—backgrounds which can only be reduced through the imposition of stringent

*dienes@email.arizona.edu
†shufang@email.arizona.edu
‡bthomas@physics.carleton.ca

event-selection criteria. While such cuts are often critical for signal extraction, they can have unintended consequences for distribution-based searches. Specifically, the cuts imposed on one variable can potentially distort the shapes of the kinematic distributions of other variables whenever those variables are nontrivially correlated. Such effects are not particularly important in "bump-hunting" searches, in which the goal is merely to identify an excess in the total number of observed events over the expected background. By contrast, in distribution-based searches, these effects can obscure critical information and lead to misleading results—or, in certain cases, can actually amplify distinctive features which point toward different kinds of dark-sector nonminimality. These issues are especially relevant for collider searches, wherein a variety of different strategies often exist for extracting signal from background in any particular channel.

Of course, we are not the first to study such correlations, nor are we the first to exploit such correlations for phenomenological purposes—the impact of correlations between collider variables on search strategies for new physics has been studied in a variety of contexts (see, e.g., Ref. [6]). However, as we shall demonstrate, such correlations are particularly relevant for distinguishing between minimal and nonminimal dark sectors. Indeed, these sorts of correlations between collider variables are particularly important in searches for nonminimality in the dark sector because cuts on one variable imposed for the purpose of background reduction can often selectively erase the contribution from particular invisible particles, thereby making a nonminimal dark sector appear minimal. As a result, different strategies may offer very different prospects for distinguishing among different dark-matter scenarios.

Effective strategies for distinguishing nonminimality in the dark sector been developed for certain detection channels. For example, it has been shown that DDM ensembles can give rise to statistically significant deviations from the kinematic distributions associated with traditional, single-particle dark-matter candidates at colliders [7], at direct-detection experiments [8], and at cosmic-ray detectors [9]. Similar analyses have also been performed for other nonminimal dark-matter scenarios in the context of direct detection [4], indirect detection [10], and collider searches [11–14]. However, in general, it is also important to investigate the effects of correlations between kinematic variables and their impact on distribution shapes.

In this paper, we investigate the prospects for distinguishing between minimal and nonminimal dark sectors on the basis of kinematic distributions at the the CERN Large Hadron Collider (LHC). For concreteness, we focus on the dijet $+ \not{E}_T$ channel, primarily due to its kinematic simplicity and its relevance for a wide variety of new-physics scenarios, including supersymmetry, theories with universal extra dimensions, and theories including scalar leptoquarks. Nevertheless, we emphasize that many of our findings transcend this particular analysis and apply more broadly to any distribution-based search for dark-sector nonminimality.

This paper is organized as follows. In Sec. II, we introduce the class of minimal and nonminimal dark-matter models which will serve as benchmarks in our study. In Sec. III, we then review the properties of various kinematic variables which can be constructed for the dijet $+ \not{E}_T$ channel. We examine the kinematic distributions of these variables for both our minimal and nonminimal benchmark models and determine the degree to which each variable is sensitive to the structure of the dark sector. In Sec. IV, we proceed to examine the correlations between these different variables and provide a qualitative assessment of how cuts on certain variables affect the distributions of other variables. In Sec. V, we combine our results in order to assess the extent to which signal-event distributions can be used to differentiate DDM ensembles from traditional dark-matter candidates. Finally, in Sec. VI, we conclude with a discussion of how to extend our analysis of cuts and correlations among collider variables to other channels relevant for the detection and differentiation of dark-matter candidates.

Before proceeding, one final comment is in order. Our primary aim in this paper is to examine the information that different kinematic variables can provide about the structure of the dark sector and to assess the impact of correlations between these variables. In particular, it is not our aim to present an exhaustive quantitative analysis of the discovery prospects for dark-sector nonminimality in the dijet $+ \not{E}_T$ channel. For this reason, we choose to focus on the signal contributions to the event rate and treat the SM backgrounds merely as a motivation for the cuts we impose on the signal distributions. However, we note that substantial residual backgrounds from processes such as $\bar{t}t +$ jets, $W^{\pm} +$ jets, and $Z +$ jets remain for this channel even after stringent cuts are applied. These residual backgrounds make extracting information about the dark sector particularly challenging. In Sec. VI, we shall return to this issue and discuss potential techniques for further reducing these backgrounds in future collider searches for nonminimal dark sectors. These issues notwithstanding, we emphasize that the correlations we discuss here are every bit as relevant for a full study including both signal and background contributions as they are for this background-free analysis. Moreover, many of the general considerations we discuss here transcend this particular channel and apply more broadly to any search which involves the analysis of kinematic distributions rather than merely the identification of an excess in the number of observed events.

II. PRELIMINARIES: PARAMETRIZING THE DARK SECTOR

As discussed in the Introduction, our goal is to examine the strategies and prospects for distinguishing nonminimal dark sectors on the basis of results in the dijet $+ \not{E}_T$ channel at the LHC. However, dark sectors can exhibit various degrees of nonminimality ranging from just a few dark particles all the way to large DDM-like ensembles. In order to obtain a sense of the full scope of possibilities, in this paper we shall therefore consider two extremes which sit at opposite poles of complexity.

The simplest situation one can consider is the case of a single dark-matter particle χ of mass m_χ. For concreteness, we take χ to be a Dirac fermion which transforms as a singlet under the SM gauge group. We also assume that the theory contains an additional scalar field ϕ with mass $m_\phi > m_\chi$ which transforms in the fundamental representation of $SU(3)_c$ and which can therefore be produced copiously via strong interactions at the LHC. In addition, we also assume that ϕ couples to χ and right-handed SM quarks q_R via an interaction Lagrangian of the form

$$\mathcal{L}_{\text{int}} = \sum_q [c_{\chi q}\phi^\dagger \bar{\chi} q_R + \text{H.c.}], \tag{2.1}$$

where the $c_{\chi q}$ are dimensionless coupling coefficients. For simplicity, we take the $c_{\chi q}$ to be real and focus on the case in which ϕ couples to a single light quark species, which we here take to be the up quark—i.e., we take $c_{\chi u} \equiv c_\chi$ to be nonvanishing, while $c_{\chi q} = 0$ for $q \in \{d, s, c, b, t\}$. Such coupling structures arise naturally for a variety of exotic particles in well-motivated extensions of the SM, including up squarks in flavor-aligned supersymmetry. Note that in general the $c_{\chi q}$ may be nonvanishing for either up-type or down-type quarks, depending on the $U(1)_{\text{EM}}$ charge of ϕ, but not for both simultaneously. Furthermore, we assume that there are no other interactions within this simplified model which contribute to ϕ decay, so that the decay process $\phi \to q\bar{\chi}$ dominates the width Γ_ϕ of ϕ. This situation arises naturally in any scenario in which there exists a symmetry under which ϕ and χ transform nontrivially but all SM particles transform trivially, thereby rendering χ stable. Finally, we assume that the characteristic time scale τ_ϕ associated with this decay process is sufficiently short ($\tau_\phi \lesssim 10^{-12}$ s) that ϕ decays promptly within a collider detector once it is produced.

At the opposite extreme of nonminimality, we shall consider a benchmark scenario in which the dark sector consists of an entire ensemble of individual components—e.g., an entire so-called "DDM ensemble" [5]. Indeed, in this paper such DDM ensembles will be taken as our canonical representatives of highly nonminimal dark sectors. The class of DDM models on which we choose to focus is that in which the constituent particles χ_n of this ensemble, $n = 1, \ldots, N$, are SM-gauge-singlet Dirac fermions with a mass spectrum of the form

$$m_n = m_0 + n^\delta \Delta m, \tag{2.2}$$

where the mass m_0 of the lightest constituent in the ensemble, the mass-splitting parameter Δm, and the power-law index δ are free parameters of the theory. Note that in this parametrization, $\Delta m > 0$ and $\delta > 0$ by construction, so that the index n labels the χ_n in order of increasing mass. Indeed, it turns out that many naturally occurring DDM ensembles have mass spectra of this form.

Just as for the single-component case discussed above, we also assume that the theory includes an additional, heavy scalar field ϕ with mass m_ϕ which transforms in the fundamental representation of the SM $SU(3)_c$ gauge group. Likewise, the χ_n are assumed to couple to this heavy scalar and to right-handed quarks q_R via the interaction Lagrangian

$$\mathcal{L}_{\text{int}} = \sum_{n=0}^{N} \sum_q [c_{nq}\phi^\dagger \bar{\chi}_n q_R + \text{H.c.}]. \tag{2.3}$$

Indeed, this is the analogue of the interaction Lagrangian in Eq. (2.1) for the single-particle case, and the c_{nq} are a set of dimensionless coupling coefficients analogous to c_χ. Once again, to facilitate direct comparison with the single-particle case, we focus on the case in which the c_{nq} are real and in which only $c_{nu} \equiv c_n$ is nonvanishing for each n, while $c_{nq} = 0$ for all other quark species. We also likewise assume that decay processes of the form $\phi \to q\bar{\chi}_n$ dominate Γ_ϕ to such an extent that all other contributions to that width can safely be neglected, and that all such decay processes occur promptly within the detector. Finally, we assume that the c_n scale across the ensemble according to a power-law relation of the form

$$c_n = c_0 \left(\frac{m_n}{m_0}\right)^\gamma, \tag{2.4}$$

where the exponent γ is another free parameter of the theory.

In general, the number of dark-matter components in the ensemble can be quite large, and it is possible for the masses of the heaviest components in the ensemble to greatly exceed m_ϕ. However, only those states χ_n with $m_n < m_\phi$ can be produced through the decays of ϕ, and thus only those states will be relevant for the study in this paper. As a result, for the purposes of this study, we shall effectively consider N to be the number of states in the ensemble with masses less than m_ϕ, with the understanding that $m_N < m_\phi$ but $m_{N+1} \geq m_\phi$.

We emphasize that we have chosen to focus on a scenario in which ϕ is a Lorentz scalar and transforms in the fundamental representation of $SU(3)_c$ merely for concreteness. Similar results will emerge in any alternative scenario in which ϕ transforms under the Lorentz and $SU(3)_c$ groups in such a way that two-body decays to a SM quark or gluon and one of the χ_n are permitted and dominate Γ_ϕ. For example, the results obtained for an $SU(3)_c$-octet fermion whose width is dominated by decays of the form $\phi \to g\chi_n$, where g denotes a SM gluon, are quite similar to those we obtain in this paper. Moreover, the enhanced pair-production cross section in this case would improve the prospects for distinguishing dark-sector nonminimality. Similar results would likewise emerge for different assignments of the coupling coefficients c_{nq}.

III. PROBING THE DARK SECTOR: VARIABLES THAT DO, AND VARIABLES THAT DO NOT

In this section, we survey some of the kinematic variables in common use for the event topology discussed in Sec. II, with an eye towards assessing their possible utility in probing nonminimal dark sectors. As discussed in the Introduction, bump-hunting is not enough—we need to analyze the shapes of the *distributions* associated with these variables. In this connection, several questions emerge. For instance, is it possible to distinguish nonminimal or multicomponent dark sectors from traditional single-component dark sectors on the basis of such distributions? If so, which kinematic variables provide the best prospects for doing this? In short, we seek to understand the extent to which differences in the particle content of the dark sector can affect the shapes of the kinematic distributions of whatever useful variables can be constructed.

In this section, we take the first step toward answering these questions by examining the qualitative features associated with the kinematic distributions of different variables and assessing to what extent these features are affected by dark-sector nonminimality. We begin by enumerating the kinematic variables we consider in this study and discussing their general properties. We then discuss the underlying methodology and assumptions inherent in our calculation of the corresponding kinematic distributions using Monte Carlo techniques. Finally, we present the results of this calculation and provide a preliminary assessment as to which variables have distributions which are sensitive to nonminimality, and which do not.

A. Kinematic variables

As discussed in the Introduction, one of the challenges of extracting information about the dark sector from the dijet $+\not{E}_T$ channel is the paucity of information contained in the description of any given event. Indeed, other than variables that characterize the angular size and substructure of the two jets (considerations which are not particularly relevant for this analysis), such events are completely characterized by only six independent degrees of freedom: the six components of the momenta $\vec{p}_1$ and $\vec{p}_2$ of the jets j_1 and j_2, respectively. Nevertheless, a number of kinematic variables can be constructed from these six degrees of freedom which can be used to extract information from this channel. These include

- the magnitude $\not{E}_T$ of the missing transverse momentum in the event;
- the magnitudes p_{T_1} and p_{T_2} of the transverse momenta of the leading jet j_1 and next-to-leading jet j_2 in the event, respectively, where the jets are ranked by p_T;
- the scalar sum $H_{T_{jj}}$ of the transverse momenta p_{T_1} and p_{T_2};
- the scalar sum H_T of $\not{E}_T$ and the transverse momenta p_{T_1} and p_{T_2};
- the absolute value $|\Delta\phi_{jj}|$ of the angle between j_1 and j_2;
- the variable $\alpha_T \equiv p_{T_2}/m_{jj}$, where m_{jj} is the invariant mass of j_1 and j_2 (this variable was introduced in Ref. [15] and is correlated with the degree to which these two leading jets are back to back);
- the transverse mass M_{T_1} constructed from $\vec{p}_{T_1}$ and the total missing-transverse-momentum vector $\vec{\not{p}}_T$; and
- the standard M_{T2} variable [16].

The last variable, M_{T2}, will play a significant role in this paper. We therefore pause to discuss its definition and properties in some detail. This quantity is essentially a generalization of the transverse-mass variable for use in situations in which more than one invisible particle is present in the final state for a given collider process. For the process $pp \to \phi^\dagger\phi \to jj\chi_a\bar{\chi}_b$, which is the primary focus of this study, this variable is defined as

$$M_{T2}^2(\tilde{m}) \equiv \min_{\vec{\not{p}}_{T_a}+\vec{\not{p}}_{T_b}=\vec{\not{p}}_T} [\max\{(M_T^2)_{1a}, (M_T^2)_{2b}\}], \qquad (3.1)$$

where $\tilde{m}$ is a common "trial mass" which is assumed for *both* χ_a and χ_b; where $\vec{p}_{T_1}$ and $\vec{p}_{T_2}$ are the transverse momenta of the two leading lets (ranked by p_T); where $\vec{\not{p}}_T$ is the total missing-transverse-momentum vector for the event; where $\vec{\not{p}}_{T_a}$ and $\vec{\not{p}}_{T_b}$ represent possible partitions of this total missing-transverse-momentum vector between the two invisible particles χ_a and χ_b; and where

$$(M_T^2)_{1a} \equiv m_{j_1}^2 + \tilde{m}^2 + 2(E_{T_{j_1}}\not{E}_{T_a} - \vec{p}_{T_1}\cdot\vec{\not{p}}_{T_a}),$$
$$(M_T^2)_{2b} \equiv m_{j_2}^2 + \tilde{m}^2 + 2(E_{T_{j_2}}\not{E}_{T_b} - \vec{p}_{T_2}\cdot\vec{\not{p}}_{T_b}) \qquad (3.2)$$

are the squared transverse masses of j_1 with χ_a and of j_2 with χ_b for any particular such partition, respectively. In this expression, m_{j_1} and m_{j_2} denote the masses of the two jets (which are negligible in practice). In the toy model considered here, in which only light quarks appear in the final state, we take $m_{j_1} = m_{j_2} = 0$. However, we explicitly retain the jet masses in the formulas displayed here for sake of generality. Note that by construction, the transverse energies $\not{E}_{T_{a,b}} \equiv (|\vec{\not{p}}_{T_{a,b}}|^2 + \tilde{m}^2)^{1/2}$ appearing in Eq. (3.2) are both defined in terms of the trial mass $\tilde{m}$. The M_{T2} variable in Eq. (3.1) is defined to be the minimum of the greater of these two transverse masses over all possible partitions of $\vec{\not{p}}_T$ between $\vec{\not{p}}_{T_a}$ and $\vec{\not{p}}_{T_b}$.

In cases in which each of the two decay chains in the event includes only one visible-sector particle in the final state, it can be shown [16–18] that the partition of $\vec{\not{p}}_T$ for which this minimum occurs is always the so-called "balanced" solution—i.e., the solution for which $(M_T^2)_{1a} = (M_T^2)_{2b}$. For this balanced solution, one finds that

$$M_{T2}^2(\tilde{m}) = \tilde{m}^2 + A + (A^2 - m_{j_1}^2 m_{j_2}^2)^{1/2} \times \left(1 + \frac{4\tilde{m}^2}{2A - m_{j_1}^2 - m_{j_2}^2}\right)^{1/2}, \qquad (3.3)$$

where

$$A \equiv E_{T_1} E_{T_2} + \vec{p}_{T_1} \cdot \vec{p}_{T_2}. \qquad (3.4)$$

One particularly useful feature of the M_{T2} variable is that it is bounded from above. Indeed, the maximum possible value M_{T2} can attain within any sample of events is the one in which all of the particles involved are maximally transverse, and the transverse mass reconstructed for each of the two decay chains in the event coincides with its corresponding invariant mass. It therefore follows that in traditional dark-matter models, for which $m_a = m_b = m_\chi$ by assumption, the maximum possible value $M_{T2}^{\max}$ for M_{T2} is equal to the mass m_ϕ of the parent particle. However, since the value of m_χ is in general not *a priori* known, one can only examine the functional dependence of $M_{T2}^{\max}$ on $\tilde{m}$.

In DDM scenarios, in which the masses m_a and m_b of the invisible particles associated with the two decay chains in a given event are not necessarily equal, the M_{T2} values obtained for a population of signal events in the $pp \to jj + \not{E}_T$ channel may differ significantly from those obtained in traditional dark-matter models, even for the same m_ϕ. Moreover, we emphasize that the kinematic endpoint $M_{T2}^{\max}$ itself is not particularly useful in discriminating between DDM ensembles and traditional dark-matter candidates; rather, it is only by comparing the *shapes* of the full M_{T2} distributions that one might hope to distinguish DDM ensembles from traditional dark-matter candidates. Of course, the maximum value of M_{T2} for a DDM ensemble is obtained for $m_a = m_b = m_0$, with all final-state particles maximally transverse. Thus, for a sufficiently large sample of events, one finds that $M_{T2}^{\max}(m_0) \to m_\phi$, a result identical to that obtained for a traditional dark-matter candidate with $m_\chi = m_0$.

We emphasize that the list of kinematic variables we have presented in this section is by no means complete. Indeed, a number of additional collider variables have been developed to extract information from channels involving substantial $\not{E}_T$. These include ratios of the transverse energies of visible particles [19], the so-called "constransverse mass" and variants thereof [20], and numerous generalizations of the M_{T2} variable [21], including particular variants [11] specifically designed for probing scenarios in which the invisible particles have unequal masses. While we do not consider any of these additional variables in this paper, we note that an analysis of the extent to which their kinematic distributions may be influenced by different sets of event-selection criteria would be completely analogous to the procedure outlined here.

B. Calculating distributions

Our ultimate goal is to examine the prospects these kinematic variables proffer for distinguishing between different dark sectors at the LHC. As discussed in the Introduction, an analysis of the full *distributions* associated with these kinematic variables is frequently required for this purpose. Thus, using Monte Carlo simulations, we explicitly derive kinematic distributions for these variables for both the traditional dark-matter candidates and the DDM ensembles included in this study.

Specifically, all data sets used in this study were generated at the parton level using MadGraph 5/MadEvent 1.4.8 [22] with model files obtained from the FeynRules [23] package as inputs. Events were generated at a center-of-mass energy $\sqrt{s} = 14$ TeV. For this preliminary, parton-level study, only events with two jets were generated and we did not include the effects of initial-state or final-state radiation. In order to account for the effects of detector uncertainties, we have smeared the original values for the magnitude p_T of the transverse momentum, the azimuthal angle ϕ, and the pseudorapidity η obtained for each jet in each parton-level data set according to the following procedure. We replace the value of each of these three jet parameters with a pseudorandom value distributed according to a Gaussian probability-distribution function. We take the mean value for this Gaussian function to be the original value obtained from the Monte Carlo simulation and the variance to be the square of the uncertainty in the measurement of the corresponding variable. In particular, we take the uncertainty in the p_T of each jet to be given by the jet-p_T resolution for the CMS detector. This resolution was evaluated in Ref. [24] as a function of p_T and is well approximated by the expression

$$\delta p_T(p_T) \approx 0.037 + 0.67 \times \left(\frac{p_T}{\text{GeV}}\right)^{-1/2}. \qquad (3.5)$$

We likewise take the uncertainties in η and ϕ to be given by the pseudorapidity and azimuthal-angle resolutions of the CMS detector, respectively. These resolutions were evaluated as functions of p_T in Ref. [25]. We find that the results are well approximated by the expressions

$$\delta\eta(p_T) \approx 0.024 + 3.00 \times \left(\frac{p_T}{\text{GeV}}\right)^{-3/2} + 0.070 \times \left(\frac{p_T}{\text{GeV}}\right)^{-1/2},$$
$$\delta\phi(p_T) \approx 0.027 + 2.45 \times \left(\frac{p_T}{\text{GeV}}\right)^{-1} - 0.046 \times \left(\frac{p_T}{\text{GeV}}\right)^{-1/2} \qquad (3.6)$$

for $p_T \lesssim 1$ TeV.

In addition to the above smearing, we also incorporate a set of precuts into our analysis. In particular, we consider in our analysis only those events in each of these data sets which satisfy the following precuts, which are designed to mimic a realistic detector acceptance:

- A transverse momentum $p_{T_j} \geq 40$ GeV and pseudorapidity $|\eta_j| \leq 3$ for each of the two highest-p_T jets in the event.
- A minimum separation $\Delta R_{jj} \geq 0.4$ between those two leading jets, where $\Delta R_{jj} \equiv \sqrt{(\Delta\eta_{jj})^2 + (\Delta\phi_{jj})^2}$.

Note that these acceptance cuts alone do not guarantee that a particular event satisfies any particular detector trigger. Indeed, we have chosen not to incorporate any particular triggering criteria into our precuts because different event-selection strategies may in principle be constructed around different triggers, and we wish to inject as little prejudice as possible about the event-selection strategy at this stage in the analysis. However, when we turn to assess the prospects for distinguishing DDM ensembles from traditional dark-matter candidates in Sec. V, we shall include additional cuts designed to satisfy triggering requirements.

C. Kinematic distributions

Following the above procedures, we can now evaluate the distributions associated with each of our kinematic variables.

We begin by considering the distributions associated with the variables α_T, $|\Delta\phi_{jj}|$, and $H_{T_{jj}}$. Indeed, these variables are of particular relevance for new-physics searches in the dijet $+ \not{E}_T$ channel because cuts on these variables are particularly effective in reducing SM backgrounds from QCD processes, electroweak processes, etc. In the left panel of Fig. 1, we display the α_T distributions associated with a number of traditional dark-matter models characterized by different values of m_χ, as well as the distributions associated with a number of DDM ensembles characterized by different values of γ for fixed $m_0 = 100$ GeV, $\Delta m = 50$ GeV, and $\delta = 1$. Note that these distributions have been normalized so that the total area under each is unity. In the center panel of this figure, we display the $|\Delta\phi_{jj}|$ distributions corresponding to the same parameter choices. The results shown in these two panels suggest that the shapes of α_T and $|\Delta\phi_{jj}|$ distributions are not particularly sensitive to the structure of the dark sector and therefore not particularly useful for distinguishing among different dark-matter scenarios. Indeed, we find that the α_T and $|\Delta\phi_{jj}|$ distributions obtained for different choices of the DDM model parameters m_0, Δm, and δ do not differ significantly from the distributions shown in Fig. 1.

In the right panel of Fig. 1, we display the $H_{T_{jj}}$ distributions associated with the same set of traditional dark-matter models and DDM ensembles as in the left and center panels. In contrast to the corresponding α_T and $|\Delta\phi_{jj}|$ distributions, which are largely insensitive to the structure of the dark sector, the $H_{T_{jj}}$ distributions shown in Fig. 1 display a somewhat greater sensitivity to the spectrum of masses and couplings of the invisible particles. However, despite this sensitivity, we also find that for any given DDM ensemble, there is generally a traditional dark-matter candidate with some value of m_χ which yields a fairly similar $H_{T_{jj}}$ distribution.

We now turn to the distributions associated with the kinematic variables $\not{E}_T$ and M_{T2}. The distributions of these two variables exhibit similar features. One of the reasons for this similarity is that in the limit in which both visible particles are massless, the value of M_{T2} obtained with $\tilde{m} = 0$ represents the minimum possible value for $\not{E}_T$ in any given event. Indeed, for this choice of trial mass and $m_{j_1} \approx m_{j_2} \approx 0$, Eq. (3.3) reduces to

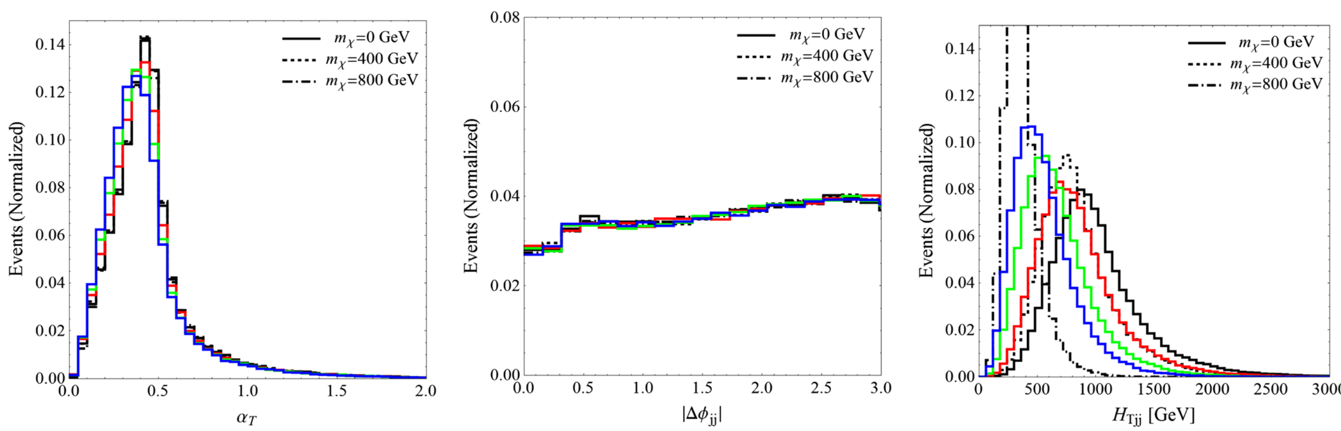

FIG. 1 (color online). A comparison of the normalized α_T (left panel), $|\Delta\phi_{jj}|$ (center panel), and $H_{T_{jj}}$ (right panel) distributions associated with traditional dark-matter candidates as well as DDM ensembles. In each panel, the black curves correspond to distributions for a representative set of traditional dark-matter candidates, while the red, green, and blue curves in each panel correspond to DDM ensembles with $m_0 = 200$ GeV, $\Delta m = 50$ GeV, $\delta = 1$, and $\gamma = \{0, 1, 2\}$, respectively. All distributions shown correspond to a parent-particle mass $m_\phi = 1$ TeV.

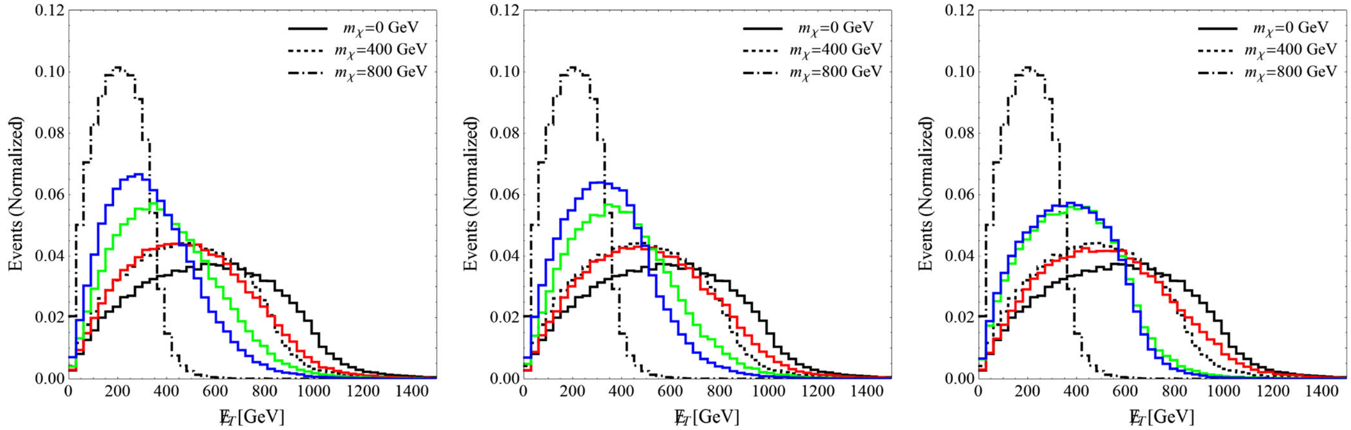

FIG. 2 (color online). A comparison of the normalized $\not{E}_T$ distributions associated with traditional dark-matter candidates as well as DDM ensembles. In each panel, the black curves correspond to distributions for a representative set of traditional dark-matter candidates, while the colored curves in the left, middle, and right panels correspond to the DDM parameter choices $m_\phi = 1$ TeV, $m_0 = 200$ GeV, $\delta = 1$, and $\Delta m = \{50, 300, 500\}$ GeV, respectively, with $\gamma = 0$ (red), $\gamma = 1$ (yellow), and $\gamma = 2$ (blue).

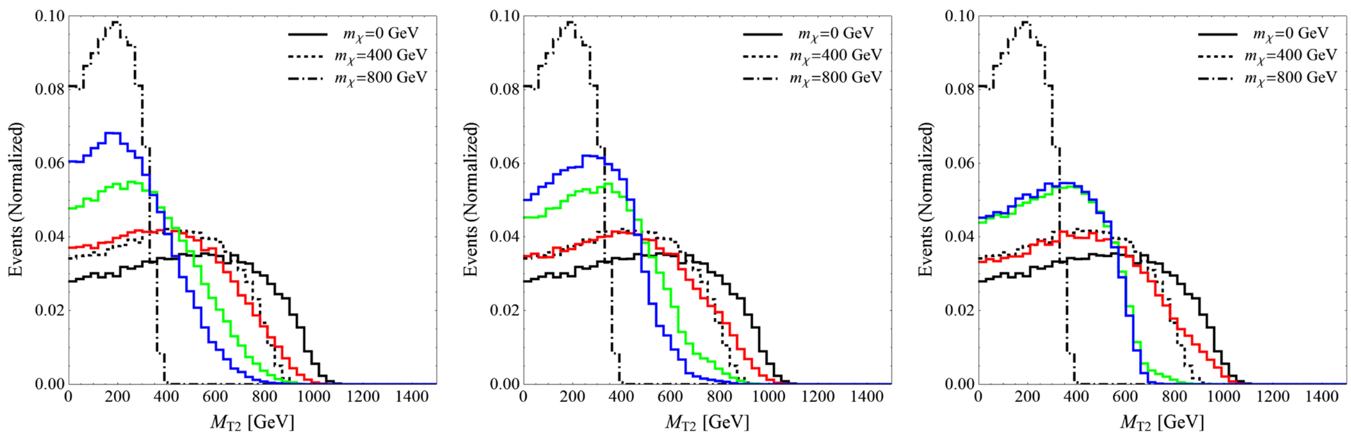

FIG. 3 (color online). Same as Fig. 2, but for normalized M_{T2} distributions with trial mass $\tilde{m} = 0$.

$$M_{T2}^2(0) \approx 2A \approx 2(E_{T_1}E_{T_2} + \vec{p}_{T_1} \cdot \vec{p}_{T_2}). \tag{3.7}$$

Likewise, in this same limit, $\not{E}_T^2$ reduces to

$$\begin{aligned} \not{E}_T^2 &= (\vec{p}_{T_1} + \vec{p}_{T_2})^2 \\ &\approx E_{T_1}^2 + E_{T_2}^2 + 2\vec{p}_{T_1} \cdot \vec{p}_{T_2}. \end{aligned} \tag{3.8}$$

The minimum value of $\not{E}_T$ is obtained for $E_{T_1} = E_{T_2}$, for which $\not{E}_T = M_{T2}(0)$. This relationship between $\not{E}_T$ and M_{T2} results in the distributions of these two variables being quite similar within any particular dark-matter model. However, despite this similarity, there are also slight but important differences between these two distributions (i.e., differences in their precise kinematic endpoints and slopes, the sharpness of their individual features, etc.). Moreover, as we shall see, these differences between these two distributions lead to a difference in their sensitivities to nonminimality in the dark sector after cuts are applied.

In Fig. 2, we display the normalized $\not{E}_T$ distributions associated with a number of traditional dark-matter models characterized by different values of m_χ as well as a number of DDM ensembles characterized by different values of the parameters m_0, Δm, and γ (with $\delta = 1$). In contrast to the distributions for α_T and $|\Delta\phi_{jj}|$ displayed in Fig. 1, the $\not{E}_T$ distributions shown in Fig. 2 are far more sensitive to the structure of the dark sector. Events which involve the heavier χ_n in a DDM ensemble tend to have smaller $\not{E}_T$ values. The contribution from such events therefore tends to shift the peak of the distribution to lower $\not{E}_T$—especially when γ is large and the branching fraction of ϕ to the heavier kinematically accessible χ_n in the ensemble is sizeable. On the other hand, the contribution from the lighter χ_n nevertheless affects the "tail" of the distribution at high $\not{E}_T$. The interplay between these two effects results in distributions for DDM ensembles with shifted peaks and longer tails—distributions whose distinctive shapes are not reproduced by any traditional dark-matter candidate, regardless of the value of m_χ. Moreover, it can also be seen from Fig. 2 that the shape of the $\not{E}_T$ distribution associated with a DDM ensemble is also sensitive to the choice of DDM model parameters. Indeed, as discussed above, larger values of γ serve to shift the peak of the distribution to lower $\not{E}_T$. Furthermore, comparing results across the three panels shown in the figure, we also see that larger values of Δm result in a sharp decrease in event count with increasing $\not{E}_T$ above the value for which the distribution peaks, whereas smaller values of Δm result in a more gradual decline in event count with increasing $\not{E}_T$.

Finally, in Fig. 3, we display the M_{T2} distributions associated with a variety of DDM ensembles for the trial mass $\tilde{m} = 0$. Note that this choice of $\tilde{m}$ generally yields the most distinctive distributions because the M_{T2} variable is restricted to the range $\tilde{m} \leq M_{T2}(\tilde{m}) \leq m_\phi$ for any particular choice of $\tilde{m}$. Thus, as $\tilde{m}$ increases, the window of possible M_{T2} values narrows and the resulting distributions become more "compressed" and therefore less distinctive.

Once again, just as with the $\not{E}_T$ distributions shown in Fig. 2, we find that the M_{T2} distributions shown in this figure display a significant sensitivity to the structure of the dark sector. Moreover, the shapes of the distributions of these two variables depend on the DDM model parameters in similar ways. For example, the shapes of the M_{T2} distributions associated with DDM ensembles with larger values of γ peak at lower values of M_{T2} while still retaining a significant tail which extends out to the kinematic endpoint at $M_{T2}^{\max} = m_\phi$. For large Δm, the individual contributions to the distributions from events with different values of m_a and m_b can be independently resolved, as shown in the right panel of the figure, and a "kink" behavior arises similar to that which arises in the case in which multiple invisible particles are produced from a single decay chain [13]. By contrast, for small Δm, these contributions cannot be resolved, and the tail of the resulting distribution appears smooth. In either case, it is evident from Fig. 3 that M_{T2} distributions are particularly useful for distinguishing DDM ensembles from traditional dark-matter candidates—and from each other. In fact, as we shall show in Sec. V, M_{T2} is an even better variable than $\not{E}_T$ for extracting information about the structure of the dark sector.

The distributions associated with the other kinematic variables discussed above (including p_{T_1}, p_{T_2}, H_T, and the transverse mass M_{T_1}) likewise display some sensitivity to the structure of the dark sector. However, we find that these distributions have far less power for distinguishing minimal from nonminimal dark sectors than those associated with $\not{E}_T$ and M_{T2}. Moreover, these variables also turn out to be less effective than α_T, $|\Delta\phi_{jj}|$, and $H_{T_{jj}}$ for extracting signal from background. Thus, we shall not consider the distributions of these other variables further.

In summary, we conclude that the distributions of some kinematic variables, such as α_T and $|\Delta\phi_{jj}|$, are almost completely insensitive to the degree of nonminimality of the dark sector. By contrast, we find that others, such as $\not{E}_T$ and M_{T2}, are particularly sensitive to such nonminimality. Finally, we find that still others, such as $H_{T_{jj}}$, lie between these two extremes.

IV. CORRELATIONS BETWEEN KINEMATIC VARIABLES

In any experiment, signals come with unwanted backgrounds. Finding cuts that reduce these backgrounds relative to the resulting signal is therefore an important task. Although we are not performing a detailed analysis of the backgrounds in this paper, there are certain SM backgrounds which are endemic to dark-matter searches in this channel. Along with these are certain cuts which are well known to be particularly advantageous in dealing with these backgrounds.

For example, cuts on variables such as α_T and $|\Delta\phi_{jj}|$—variables which are strongly correlated with the angle between the spatial momenta $\vec{p}_{T_1}$ and $\vec{p}_{T_2}$ of the two leading jets in a given event—are particularly effective in reducing the substantial QCD background in the dijet $+ \not{E}_T$ channel. This is because QCD-background events tend to be back-to-back and therefore seldom have $\alpha_T \gtrsim 0.5$. Indeed, the minimum cut $\alpha_T > 0.55$ imposed in CMS searches in this channel [26,27] has been shown to be extremely effective in reducing—and indeed effectively eliminating—the sizeable background from QCD processes.

Likewise, cuts on variables such as $H_{T_{jj}}$ and H_T—variables which are correlated with the overall energy of the underlying event—can be effective in reducing the remaining SM backgrounds which are dominated by processes such as $\bar{t}t +$ jets, $W^\pm +$ jets with the $W^\pm$ decaying leptonically, and $Z +$ jets with the Z decaying into a neutrino pair. These variables are relevant for searches in the dijet $+ \not{E}_T$ channel for another reason as well: detector triggers useful in selecting events involving hadronic jets and substantial $\not{E}_T$ frequently rely on the scalar sum of the transverse momenta of those jets exceeding a particular threshold.

Unfortunately, it is possible for cuts on these variables to significantly affect the shapes of the distributions we have calculated in Sec. III. Such cuts might therefore eliminate not only our backgrounds, but also the ability of kinematic variables such as $\not{E}_T$ and M_{T2} to discriminate between minimal and nonminimal dark sectors. To illustrate this possibility, we can begin with the $\not{E}_T$ and M_{T2} distributions in Figs. 2 and 3 and impose a single additional cut $\alpha_T > 0.55$. The results are shown in Figs. 4 and 5. Note that although this cut also results in a substantial reduction in the signal-event count, our primary focus is on the *shapes* of the distributions. Thus, the distributions in Figs. 4 and 5 are likewise normalized so that the area under each distribution is unity.

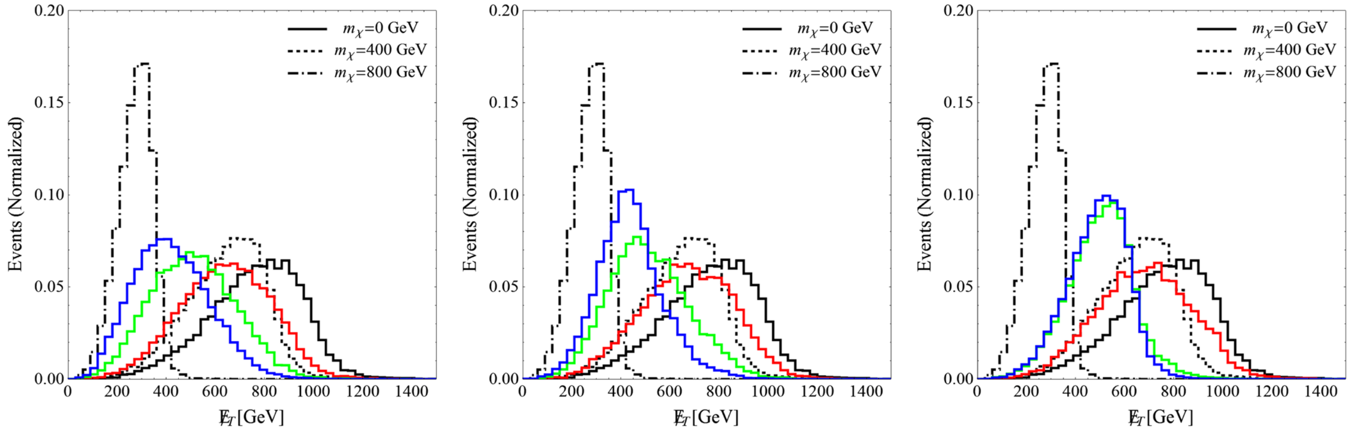

FIG. 4 (color online). Same as Fig. 2, but with the additional cut $\alpha_T > 0.55$.

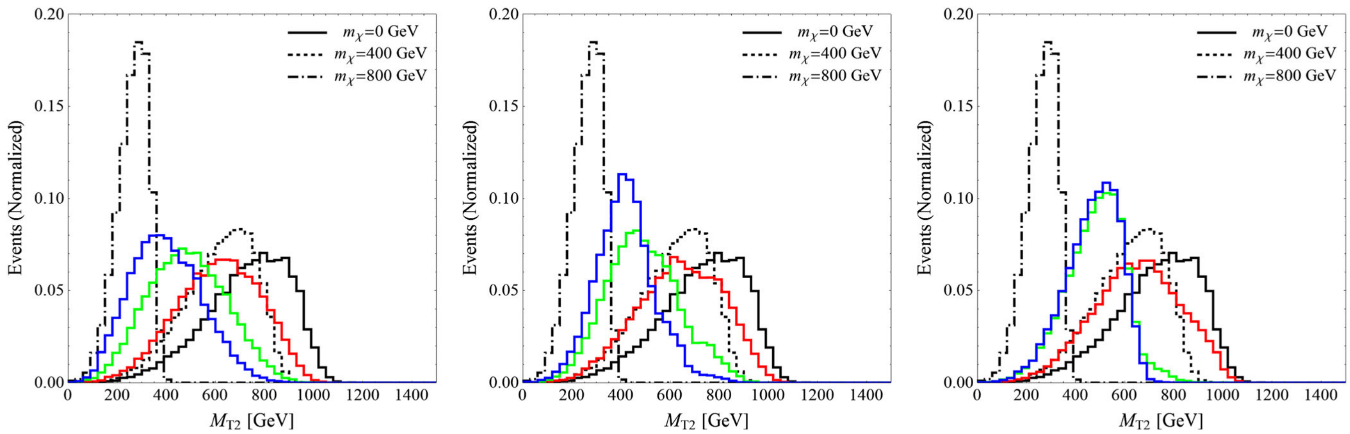

FIG. 5 (color online). Same as in Fig. 3, but with the additional cut $\alpha_T > 0.55$.

Comparing the distributions in Fig. 4 with those of Fig. 2 (or equivalently comparing those of Fig. 5 with those of Fig. 3), we see that our α_T cut has had a significant impact on the shapes of these $\not{E}_T$ and M_{T2} distributions. Such cuts can therefore have a significant effect on our ability to distinguish minimal from nonminimal dark sectors. Indeed, this is true even when the variable on which the cut is imposed itself displays little sensitivity to the parameters which characterize the dark sector—as we have shown to be the case for α_T.

Ultimately, cuts on variables such as α_T and $H_{T_{jj}}$ are able to affect the shapes of $\not{E}_T$ and M_{T2} distributions for only one reason: *there are nontrivial correlations between these two groups of variables*. Otherwise, in the absence of such correlations (and given sufficient statistics), cuts on these variables would result in a uniform reduction in signal events across these distributions but leave the overall *shapes* of these distributions intact.

In order to explore this issue further, we turn to directly examine the correlations between the variables $\{\alpha_T, |\Delta\phi_{jj}|, H_{T_{jj}}\}$—which are important for removing backgrounds and extracting signals—and the variables $\{\not{E}_T, M_{T2}\}$—which are also important for distinguishing between minimal and nonminimal dark sectors. The correlations between this former set of variables and M_{T2} (with a trial mass $\tilde{m} = 0$) are illustrated in the scatter plots displayed in Fig. 6 for a benchmark set of traditional dark-matter models (left column) and DDM ensembles (center and right columns). In each of these scatter plots, we display several sets of data points associated with these different benchmark models. Each data point corresponds to a single event chosen randomly from the Monte Carlo data sample for that model: its color indicates the model with which it is associated and its coordinates indicate the values x and y of the two kinematic variables X and Y of interest for the corresponding event. Thus, the density of points within the region (x, y) to $(x + \delta x, y + \delta y)$ indicates the relative likelihood of values for X and Y within that range occurring in combination. A uniform density of points throughout a particular panel would imply that the variables are essentially uncorrelated.

Clearly, the results shown in Fig. 6 indicate not only that M_{T2} and the variables $\{\alpha_T, |\Delta\phi_{jj}|, H_{T_{jj}}\}$ are correlated in interesting, nontrivial ways, but also that these correlations often depend sensitively on the masses and couplings of the

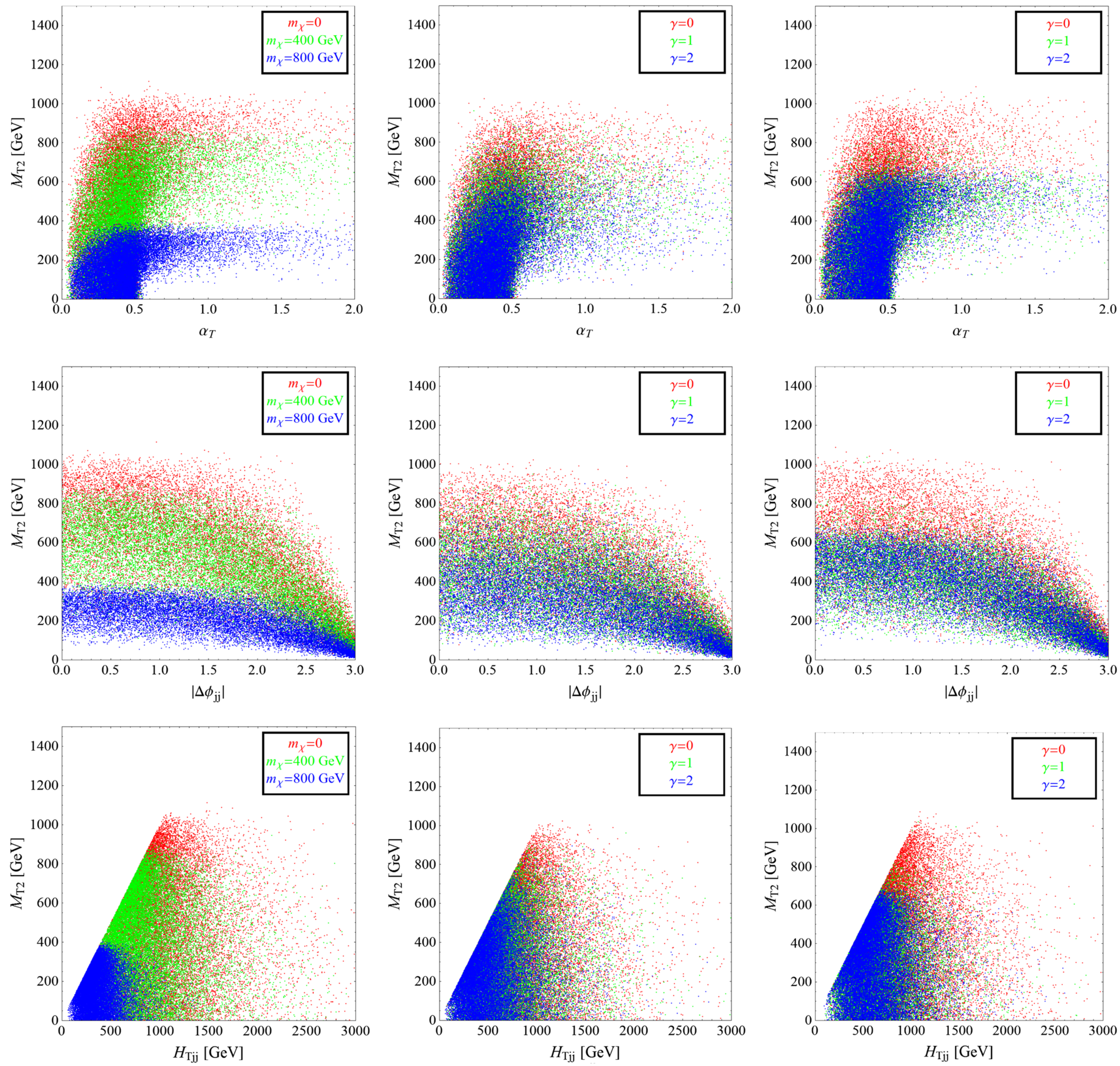

FIG. 6 (color online). Scatter plots illustrating the correlations between M_{T2} and the selection variables α_T (top row), $|\Delta\phi_{jj}|$ (center row), and $H_{T_{jj}}$ (bottom row) for a trial mass $\tilde{m} = 0$. The left panel in each row shows the results for traditional dark-matter models with $m_\chi = 0$ (red), $m_\chi = 400$ GeV (green), and $m_\chi = 800$ GeV (blue). The center panel in each row shows the results for three DDM models, with $m_0 = 100$ GeV, $\Delta m = 50$ GeV, $m_\phi = 1$ TeV, and $\gamma = 0$ (red), $\gamma = 1$ (green), and $\gamma = 2$ (blue). The right panel in each row shows the corresponding results for a DDM model with $\Delta m = 500$ GeV and all other parameters unchanged.

dark-sector particles. For example, we observe from the top left panel of this figure that there is far less overlap among the data-point distributions for traditional dark-matter models with different m_χ within the region of parameter space in which $\alpha_T > 0.55$ than there is within the region in which $\alpha_T < 0.55$. Therefore, while a cut on α_T of this magnitude does significantly reduce the total number of signal events, this effect is offset at least in part by the fact that the M_{T2} distributions of the surviving data points for different m_χ are significantly more segregated from one another after the cut than before. Indeed, the way in which α_T and M_{T2} are correlated makes α_T a particularly effective selection variable: not only are cuts on α_T effective in reducing SM backgrounds, but they also serve to *amplify* distinctions between the shapes of the M_{T2} distributions associated with different dark-matter models. Indeed, as we shall see in Sec. V, this effect more than compensates for the loss in signal-event count that arises for a threshold cut

$\alpha_T^{\min}$ on α_T of the order necessary to effectively eliminate the substantial QCD background.

It is likewise evident from Fig. 6 that similar correlations exist between $|\Delta\phi_{jj}|$ and M_{T2}. However, cuts on α_T and $|\Delta\phi_{jj}|$ are to a large extent redundant, since both variables essentially reflect the degree to which the leading two jets in a given event are back-to-back. Moreover, we note that cuts on α_T are typically found to be significantly more effective in reducing SM backgrounds than cuts on $|\Delta\phi_{jj}|$. For these reasons, we henceforth focus on α_T, but we note that results similar to those we obtain in this study could in principle be obtained by imposing cuts on $|\Delta\phi_{jj}|$ rather than α_T.

By contrast, Fig. 6 reveals that $H_{T_{jj}}$ and M_{T2} are correlated in such a way that imposing a substantial minimum cut on $H_{T_{jj}}$ distorts M_{T2} distributions in a reliable but far less advantageous manner. In particular, we observe from the bottom left panel of this figure that a minimum cut of $H_{T_{jj}}$ results in a far more severe reduction in signal events for traditional dark-matter models with large m_χ than for those with small m_χ. This in turn implies that in DDM scenarios and other theories involving multiple invisible particles, information about the heavier particles tends to be washed out by the application of such a cut. It therefore follows that DDM ensembles with extremely large values of the coupling index γ will be somewhat more difficult to distinguish on the basis of their M_{T2} distributions, since the branching fractions of the parent particle ϕ to the heavier χ_i are comparatively large in this case.

We note that while the results shown in Fig. 6 correspond to the choice of $\tilde{m} = 0$, we find that the corresponding results for other choices of this trial mass exhibit the same qualitative features. However, as discussed in Sec. III, the window of possible M_{T2} values narrows as $\tilde{m}$ increases. In general, this narrowing results in a greater degree of overlap among the the data-point distributions associated with different dark-matter models and consequently makes distinguishing among such models more difficult. We also note that in both the $\Delta m \to \infty$ and $\gamma \to -\infty$ limits, the data-point distribution associated with a DDM ensemble reduces to that associated with a single dark-matter particle with $m_\chi = m_0$, as expected.

Since we have seen in Sec. III that the shape of the $\not{E}_T$ distribution is also sensitive to the structure of the dark sector, it is interesting to examine the correlations between $\not{E}_T$ and the variables $\{\alpha_T, |\Delta\phi_{jj}|, H_{T_{jj}}\}$ as well. We find that each of these variables turns out to be correlated with $\not{E}_T$ in a manner extremely similar to that in which it is correlated with M_{T2}. Indeed, the corresponding scatter plots are qualitatively so similar to those shown in Fig. 6 that we refrain from reproducing them here. As we shall see in Sec. V, these correlations likewise imply that imposing cuts on variables such as α_T, $|\Delta\phi_{jj}|$, and $H_{T_{jj}}$ can have a significant effect on the distributions of both $\not{E}_T$ and M_{T2}.

V. COMPARING CORRELATIONS: BALANCING SIGNAL EXTRACTION AGAINST DARK-SECTOR RESOLUTION

As we have seen, the existence of nontrivial correlations between the variables $\{\alpha_T, |\Delta\phi_{jj}|, H_{T_{jj}}\}$ and the variables $\{\not{E}_T, M_{T2}\}$ implies that cuts on variables in the first set will distort the shapes of the kinematic distributions associated with variables in the second set. This is generically true for both traditional single-component dark sectors and nonminimal dark sectors. However, these correlations are ultimately a reflection of fundamental kinematic relationships between the masses, energies, and momenta of the particles involved in the production and decay processes associated with any particular event. This means that the way in which kinetic variables are correlated—and therefore the effect that a cut on one such variable will have on the distribution of another—is itself dependent on the properties of the dark-sector particles.

As a result, the degree to which we can ultimately exploit the distributions associated with the $\{\not{E}_T, M_{T2}\}$ variables in order to distinguish between any two dark-matter models—and, by extension, between minimal and nonminimal dark sectors—rests upon our understanding of the correlations that exist for those models. Indeed, in order to assess the degree to which dark-sector nonminimality can be distinguished at the LHC, we must compare the effects of the correlations which arise in nonminimal dark sectors with the effects of the correlations which arise in minimal dark sectors. More specifically, for the case at hand, we must ultimately *compare* the correlations illustrated in the second and third columns of Fig. 6 with those illustrated in the first column of Fig. 6.

In order to make this comparison, we require a method of quantifying the degree to which the expected distribution for any particular collider variable associated with a given DDM ensemble is distinct from the distributions associated with traditional dark-matter candidates in general. To do this, we shall adopt a procedure similar to that employed in Ref. [7]. In particular, we survey over a variety of traditional dark-matter candidates, each characterized by a different value of m_χ, and compare the distribution of that variable with the distribution obtained for the DDM ensemble of interest. We include in our survey values of m_χ ranging from $m_\chi = 0$ to $m_\chi = m_\phi$ at intervals of 100 GeV. For each value of m_χ, we assess the degree of distinctiveness between the two distributions by computing the goodness-of-fit statistic $G(m_\chi) \equiv -2\ln\lambda(m_\chi)$, where $\lambda(m_\chi)$ is the ratio of the likelihood functions for the two distributions. For binned data in which the number of events in each bin is independent of the number of events in every other bin, $G(m_\chi)$ takes the form

$$G(m_\chi) = 2\sum_{k=1}^{N}\left[\mu_k(m_\chi) - n_k + n_k \ln\left(\frac{n_k}{\mu_k(m_\chi)}\right)\right], \quad (5.1)$$

where the index k labels the bin, where n_k is the expected population of events in bin k in the DDM model, and where $\mu_k(m_\chi)$ is the expected population of events in bin k in the traditional dark-matter model to which this DDM model is being compared. We take the minimum value

$$G_{\min} \equiv \min_{m_\chi}\{G(m_\chi)\} \quad (5.2)$$

from among the $G(m_\chi)$ obtained in our survey over m_χ as our final measure of the distinctiveness of the distribution associated with the DDM ensemble. Moreover, for the case in which the expected population of events in each bin is sufficiently large, the $G_{\min}$ statistic follows a χ^2 distribution with $N-1$ degrees of freedom. We can therefore estimate the statistical significance of our results by comparing the value of $G_{\min}$ to such a χ^2 distribution in order to obtain a p value. We then take the number of standard deviations away from the mean to which this p value would correspond for a Gaussian distribution as an estimate of the statistical significance of differentiation—i.e., the statistical significance with which the signal distribution can be claimed to differ from the expected distributions for traditional dark-matter candidates. We note that in principle one could also incorporate a broader class of traditional dark-matter models with other particle properties and coupling structures into this survey; however, the inclusion of such additional models in our analysis will not significantly impact our results.

One subtlety which arises in quantifying the discrepancy between different kinematic distributions is that the reliability of most goodness-of-fit statistics breaks down in cases in which there are bins for which the expected number of events in the reference model is small or zero. For example, the $G(m_\chi)$ statistic defined in Eq. (5.1) is infinite if the expected number of events in one or more bins is zero in the traditional dark-matter model to which the DDM model is being compared. In order to address this issue, the event count in each bin in a given background-event distribution for which $\mu_k(m_\chi) < 3$ is treated as if it were $\mu_k(m_\chi) = 3$. This is the event count which corresponds to the 95% C.L. upper limit on the expected number of events for data which follow a Possion distribution in the case in which no events are observed [28]. Likewise, the event count in each bin in a given signal-event distribution for which $n_k < 3$ is treated as if it were $n_k = 3$. Note that while the normalization of each distribution is in principle fixed by the measurement of the total number of signal events, this procedure for treating low-statistics bins does not necessarily preserve the equality between the sum of the n_k and the sum of the $\mu_k(m_\chi)$ for any two kinematic distributions being compared. Thus, the $G(m_\chi)$ statistic for each m_χ in the survey takes the form given in Eq. (5.1), rather than the alternative form appropriate for data distributed according to a multinomial distribution.

Having defined the $G_{\min}$ statistic in Eq. (5.2), we now turn to examine how the imposition of event-selection criteria can affect the distinctiveness of the distributions of key kinematic variables—in particular, M_{T2} and $\not{E}_T$. We begin by examining the effect of imposing a minimum cut $\alpha_T^{\min}$ on α_T. In the top left panel of Fig. 7, we plot the value of $G_{\min}$ for the M_{T2} distributions associated with several DDM ensembles as a function of $\alpha_T^{\min}$. The precuts are the only additional cuts imposed on the data. The results shown here correspond to an integrated luminosity $\mathcal{L}_{\rm int} = 300\ {\rm fb}^{-1}$ at each of the LHC detectors. Note that while $G_{\min}$ generally decreases with increasing $\alpha_T^{\min}$ due to the overall reduction in number of signal events, it does not do so monotonically. Indeed, for all curves shown, $G_{\min}$ actually *rises* with increasing $\alpha_T^{\min}$ within the range $0.4 \lesssim \alpha_T^{\min} \lesssim 0.55$. As can readily be seen from Fig. 6, this is precisely the range within which the α_T cut effectively eliminates the region of parameter space within which the data-point distributions corresponding to different invisible-particle masses overlap, yet still retains the majority of the events in the region within which those data-point distributions are the most distinctive. A similar enhancement in the $G_{\min}$ values obtained from the corresponding $\not{E}_T$ distributions is apparent in the bottom left panel of Fig. 7.

We now turn to examine the effect on $G_{\min}$ of imposing a minimum cut $H_{T_{jj}}^{\min}$ on $H_{T_{jj}}$. In the top right panel of Fig. 7, we plot the value of $G_{\min}$ for the M_{T2} distributions associated with the same DDM ensembles as a function of $H_{T_{jj}}^{\min}$. Once again, the precuts are the only additional cuts imposed on the data. In contrast with the $G_{\min}$ curves for $\alpha_T^{\min}$, we see that the corresponding curves for $H_{T_{jj}}^{\min}$ fall monotonically due to the loss in statistics. This is to be expected, as we have seen that there is no advantageous correlation between $H_{T_{jj}}$ and M_{T2} which can be exploited to offset this loss. The same behavior is also apparent in the $G_{\min}$ values obtained from the corresponding $\not{E}_T$ distributions in the bottom right panel of Fig. 7.

Despite the enhancement within the range $0.4 \lesssim \alpha_T^{\min} \lesssim 0.55$ discussed above, it is nevertheless clear from Fig. 7 that increasing $\alpha_T^{\min}$ generally has the effect of diminishing our power to discriminate nonminimal dark sectors from traditional dark sectors. Likewise, we see that a similar conclusion holds, perhaps even more dramatically, for cuts on $H_{T_{jj}}$. However, the extraction of signal from background typically requires more than simply one or the other cut in isolation: we typically need to impose an entire slew of cuts simultaneously. Inevitably, these cuts, which are designed to enhance signal extraction, further reduce our power to resolve nontrivial dark sectors relative to traditional dark sectors. Thus, we find ourselves in a position in which we must ultimately balance considerations related to signal extraction against those related to dark-sector resolution.

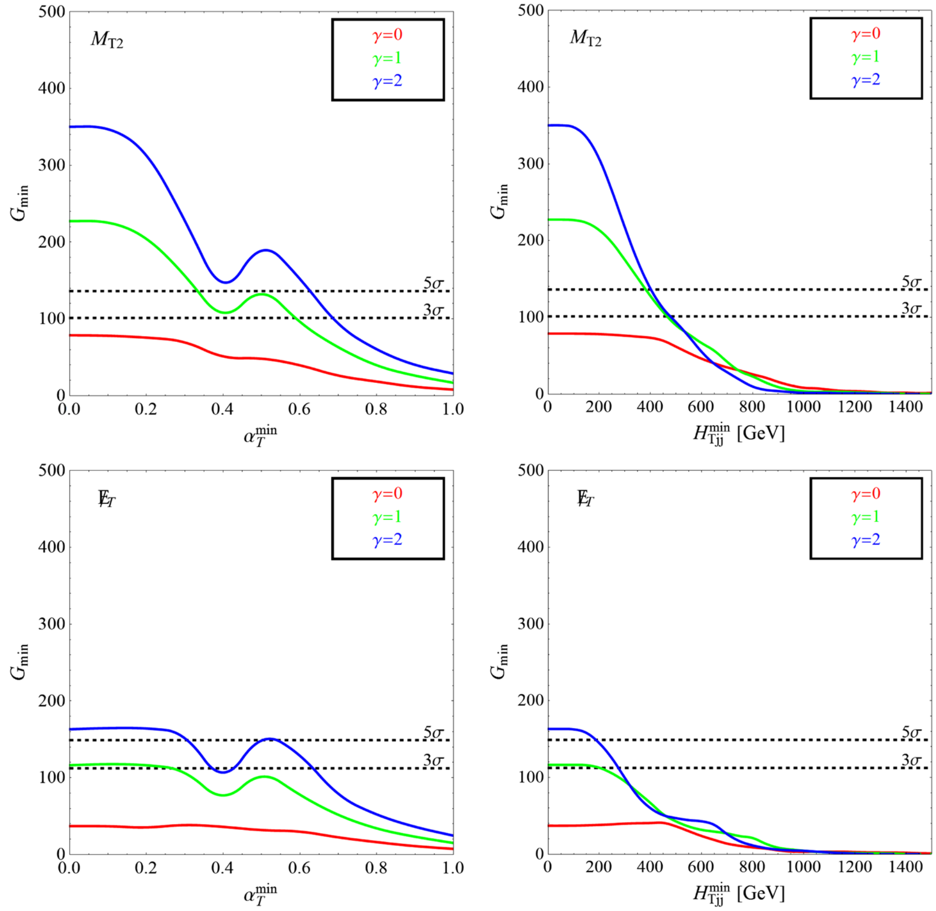

FIG. 7 (color online). The value of the statistic G_{min} for the M_{T2} distributions (top row) and $\not{E}_T$ distributions (bottom row) associated with several DDM ensembles as a function of the minimum cut α_T^{min} imposed on α_T (left column) or the minimum cut $H_{T_{jj}}^{min}$ imposed on $H_{T_{jj}}$ (right column). In each case, the precuts in Sec. III B are the only other cuts imposed on the data. The curves shown in all panels correspond to the parameter choices $m_0 = 100$ GeV, $\Delta m = 50$ GeV, and $\delta = 1$, and the M_{T2} curves correspond to a trial mass $\tilde{m} = 0$. Further details are discussed in the text.

In order to study this issue, we adopt a set of cuts which is similar to those employed in the CMS jets + $\not{E}_T$ analysis in Ref. [26]. In particular, we simultaneously require that

- $\{p_{T_{j_1}}, p_{T_{j_2}}\} \geq 100$ GeV,
- $\not{E}_T \geq 90$ GeV,
- $\alpha_T \geq 0.55$.

In addition to these cuts, we also impose a minimum cut of the form $H_{T_{jj}} \geq H_{T_{jj}}^{min}$ on the data and examine the effect of varying $H_{T_{jj}}^{min}$ on the statistical significance of differentiation between DDM and traditional dark-matter models. As discussed in Sec. IV, a cut of this sort can be effective in reducing the backgrounds from SM processes such as $t\bar{t}$ + jets, $W^{\pm}$ + jets, and Z + jets—processes which can give rise to genuine sources of missing energy in the form of neutrinos, and whose contributions to the total SM background are therefore more likely to survive the α_T cut. Note also that these selection cuts are sufficient for passing CMS triggering requirements, provided that $H_{T_{jj}}^{min} \geq 275$ GeV [26].

Our results are shown in Table I, where we display the Gaussian-equivalent significance of differentiation for the M_{T2} distributions associated with several benchmark DDM models after the imposition of the selection cuts described above. These benchmark models are characterized by different values of Δm and γ, with fixed $m_0 = 100$ GeV. Results are given for several different choices of $H_{T_{jj}}^{min}$.

The decline in sensitivity with increased $H_{T_{jj}}^{min}$ can be qualitatively understood as follows. Since events involving heavier χ_n tend to have both smaller $H_{T_{jj}}$ values and smaller M_{T2} values, as shown in the bottom left panel of Fig. 6, increasing $H_{T_{jj}}^{min}$ results in a disproportionately severe reduction in events involving heavier χ_n in comparison with events involving lighter ones. As a result, increasing $H_{T_{jj}}^{min}$ has the effect of washing out the imprints of the heavier χ_n in M_{T2} distributions and leads to a decrease in the significance of differentiation, as seen in Table I.

Similarly, the dependence of the results shown in Table I on the power-law index γ can be qualitatively understood as

TABLE I. The statistical significance of differentiation derived from examining the goodness of fit between the M_{T2} distributions associated with a variety of benchmark DDM models and those associated with traditional dark-matter models. The values of Δm and γ for each DDM model are specified in the table, and in all cases we have taken $m_0 = 100$ GeV and $\delta = 1$. The results shown here correspond to an integrated luminosity of $\mathcal{L}_{\rm int} = 300\ {\rm fb}^{-1}$ in each of the two LHC detectors for a center-of-mass energy $\sqrt{s} = 14$ TeV. The event-selection criteria imposed include the minimum cut on $H_{T_{jj}}$ shown in the table as well as the other selection cuts discussed in the text.

DDM benchmark		Significance σ			
Δm	γ	$H_{T_{jj}}^{\rm min} = 275$ GeV	$H_{T_{jj}}^{\rm min} = 325$ GeV	$H_{T_{jj}}^{\rm min} = 375$ GeV	$H_{T_{jj}}^{\rm min} = 425$ GeV
50 GeV	0	0.03	0.02	0.01	0.01
50 GeV	1	3.08	2.60	1.20	0.22
50 GeV	2	3.13	1.35	0.09	0.00
300 GeV	0	0.00	0.00	0.00	0.00
300 GeV	1	1.39	1.33	1.22	1.17
300 GeV	2	4.63	4.14	3.02	1.31
500 GeV	0	0.02	0.01	0.01	0.01
500 GeV	1	0.00	0.00	0.00	0.00
500 GeV	2	0.00	0.00	0.00	0.00

follows. As γ decreases, the width Γ_ϕ of ϕ will be increasingly dominated by the contribution from decays to the lightest dark-matter component χ_0. Thus, for sufficiently small γ, the resulting kinematic distributions become effectively indistinguishable from those obtained for a traditional dark-matter candidate of mass $m_\chi = m_0$. Conversely, for sufficiently large γ, it turns out that Γ_ϕ will be dominated by the contributions from the most massive kinematically accessible states in the ensemble. In this regime, the resulting kinematic distributions become effectively indistinguishable from those obtained for a traditional dark-matter candidate with m_χ equal to the mass of the most massive accessible ensemble component. Indeed, as was noted in Ref. [7] in the case of three-body parent-particle decays, there exists a particular intermediate range of γ for any particular assignment of m_0, Δm, etc., within which the branching fractions of ϕ to two or more of the χ_n are of roughly the same order and the corresponding kinematic distributions are therefore more distinctive.

Taken together, then, the primary message of the results shown in Table I is that there are nontrivial regions of our parameter space within which the population of signal events associated with a DDM ensemble can be distinguished from the population of signal events associated with any traditional dark-matter candidate on the basis of the distributions of kinematic variables such as M_{T2}. Indeed, with an integrated luminosity of 300 $\rm fb^{-1}$ in both LHC detectors, a statistical significance of differentiation close to 5σ is obtained for low-to-moderate values of $H_{T_{jj}}^{\rm min}$ for 50 GeV $\lesssim m_0 \lesssim$ 300 GeV and $1 \lesssim \gamma \lesssim 2$.

VI. DISCUSSION AND CONCLUSIONS

In this paper, we have investigated the prospects for distinguishing nonminimal dark sectors in the dijet $+ \not{E}_T$ channel at the LHC. Almost by necessity, searches of this sort—both in this channel and others—involve not merely identifying an excess in the total number of signal events over background, but actually analyzing the shapes of the full distributions of the relevant kinematic variables. It is therefore critical to examine the correlations between such variables, since cuts imposed on one variable in order to reduce the background have the capacity to alter or distort the distributions of other variables which are critical for probing the structure of the dark sector.

Using DDM ensembles as a benchmark, we have examined the extent to which the distributions of different kinematic variables are impacted by dark-sector nonminimality. We have shown that the distributions of certain variables such as $\not{E}_T$ and M_{T2} are particularly sensitive to the properties of the dark-sector particles. By contrast, we have shown that the distributions of other variables such as α_T and $|\Delta\phi_{jj}|$ are comparatively insensitive to the details of the dark sector. Finally, we have shown that still other variables such as $H_{T_{jj}}$ lie between these extremes.

Furthermore, we have also demonstrated that nontrivial correlations exist between the variables $\{\not{E}_T, M_{T2}\}$ and the variables $\{\alpha_T, |\Delta\phi_{jj}|, H_{T_{jj}}\}$. In particular, we find that α_T is correlated with M_{T2} and $\not{E}_T$ in such a way that a threshold cut on α_T can actually *enhance* the distinctiveness of the corresponding kinematic distributions in certain situations. Indeed, we have shown that this effect more than offsets the corresponding loss in statistics for certain values of $\alpha_T^{\rm min}$. By contrast, we find that $H_{T_{jj}}$ is correlated with these same variables in such a way that a threshold cut on $H_{T_{jj}}$ generically serves to wash out distinguishing features in the corresponding distributions.

Finally, we have investigated the impact of such cuts of the distinctiveness of the $\not{E}_T$ and M_{T2} distributions associated with our DDM ensembles, as quantified by the goodness-of-fit statistic $G_{\rm min}$. We have shown that correlations between variables give rise to a nontrivial dependence of $G_{\rm min}$ on the cuts imposed—a dependence which transcends mere issues of event count. Due in part to these effects, the signal-event distributions associated with DDM ensembles can be distinguished from those associated with traditional dark-matter candidates at a significance level approaching 5σ in many situations.

One final comment is in order. Our focus in this paper has been on the correlations between selection cuts and kinematic distributions of signal events and on the effects that such correlations have on the distinctiveness of those distributions. We have therefore focused our analysis primarily on the signal contributions from different dark-sector models alone and have only incorporated the SM backgrounds into our analysis as a motivation for the cuts imposed on certain kinematic variables. However, despite the established efficiency of the selection cuts adopted here in reducing those backgrounds [26,27] (and especially the contribution from QCD processes), we note that the residual backgrounds from $\bar{t}t+$jets, $W^{\pm}+$jets, and $Z+$jets are still quite sizeable. Nevertheless, it may be possible to isolate these residual backgrounds using other techniques. For example, both the normalization and shape of the "irreducible" background from $Z+$ jets can in principle be determined from the related process in which the Z decays into a pair of charged leptons [15]. Such information could in principle allow for a modeling of this background that would make background subtraction a viable possibility. Further reducing the $W^{\pm}+$jets background is a significantly more challenging endeavor. However, while a full analysis of the effect of selection cuts on the combined contribution from both signal and background processes to the relevant kinematic distributions is beyond the scope of this paper, we emphasize that the correlations we have investigated here are every bit as relevant for such a study as they have been for this background-free analysis.

ACKNOWLEDGMENTS

We would like to thank P. Loch for useful discussions. K. R. D. and S. S. are supported in part under DOE Grant No. DE-FG02-13ER-41976, while B. T. is supported in part by NSERC Canada. S. S. also wishes to acknowledge the hospitality of the Aspen Center for Physics, which is supported in part under NSF Grant No. PHY-1066293. The opinions and conclusions expressed herein are those of the authors, and do not represent any funding agency.

[1] For recent reviews, see, e.g., G. Jungman, M. Kamionkowski, and K. Griest, Phys. Rep. **267**, 195 (1996); K. A. Olive, arXiv:astro-ph/0301505; D. Hooper, arXiv:0901.4090; N. Weiner, "Dark Matter Theory," video lectures given at TASI 2009, http://physicslearning2.colorado.edu/tasi/tasi_2009/tasi_2009.htm; J. L. Feng, Annu. Rev. Astron. Astrophys. **48**, 495 (2010).

[2] P. A. R. Ade *et al.* (Planck Collaboration), Astron. Astrophys. **571**, A16 (2014).

[3] See, e.g., C. Boehm, P. Fayet, and J. Silk, Phys. Rev. D **69**, 101302 (2004); E. Ma, Annales Fond. Broglie **31**, 285 (2006); T. Hur, H. S. Lee, and S. Nasri, Phys. Rev. D **77**, 015008 (2008); M. Adibzadeh and P. Q. Hung, Nucl. Phys. **B804**, 223 (2008); J. L. Feng and J. Kumar, Phys. Rev. Lett. **101**, 231301 (2008); H. Sung Cheon, S. K. Kang, and C. S. Kim, Phys. Lett. B **675**, 203 (2009); J. H. Huh, J. E. Kim, and B. Kyae, Phys. Rev. D **79**, 063529 (2009); M. Fairbairn and J. Zupan, J. Cosmol. Astropart. Phys. 07 (2009) 001; K. M. Zurek, Phys. Rev. D **79**, 115002 (2009); H. Baer, M. Haider, S. Kraml, S. Sekmen, and H. Summy, J. Cosmol. Astropart. Phys. 02 (2009) 002; B. Batell, M. Pospelov, and A. Ritz, Phys. Rev. D **79**, 115019 (2009); F. Chen, J. M. Cline, and A. R. Frey, Phys. Rev. D **80**, 083516 (2009); H. Zhang, C. S. Li, Q. H. Cao, and Z. Li, Phys. Rev. D **82**, 075003 (2010); I. Cholis and N. Weiner, arXiv:0911.4954; X. Gao, Z. Kang, and T. Li, Eur. Phys. J. C **69**, 467 (2010); F. D'Eramo and J. Thaler, J. High Energy Phys. 06 (2010) 109; D. Feldman, Z. Liu, P. Nath, and G. Peim, Phys. Rev. D **81**, 095017 (2010); P. T. Winslow, K. Sigurdson, and J. N. Ng, Phys. Rev. D **82**, 023512 (2010); H. Baer, A. Lessa, S. Rajagopalan, and W. Sreethawong, J. Cosmol. Astropart. Phys. 06 (2011) 031; H. Baer, A. Lessa, and W. Sreethawong, J. Cosmol. Astropart. Phys. 01 (2012) 036; M. Aoki, M. Duerr, J. Kubo, and H. Takano, Phys. Rev. D **86**, 076015 (2012); J. Fan, A. Katz, L. Randall, and M. Reece, Phys. Dark Univ. **2**, 139 (2013); Phys. Rev. Lett. **110**, 211302 (2013); P.-H. Gu, Phys. Dark Univ. **2**, 35 (2013); M. Aoki, J. Kubo, and H. Takano, Phys. Rev. D **87**, 116001 (2013); Y. Kajiyama, H. Okada, and T. Toma, Eur. Phys. J. C **74**, 2722 (2014); C.-Q. Geng, D. Huang, and L.-H. Tsai, Phys. Rev. D **89**, 055021 (2014); Mod. Phys. Lett. A **29**, 1440003 (2014).

[4] S. Profumo, K. Sigurdson, and L. Ubaldi, J. Cosmol. Astropart. Phys. 12 (2009) 016.

[5] K. R. Dienes and B. Thomas, Phys. Rev. D **85**, 083523 (2012); **85**, 083524 (2012); **86**, 055013 (2012).

[6] R. Essig, Ph.D., Rutgers The State University of New Jersey, 2009 [http://search.proquest.com/docview/304456039/abstract].

[7] K. R. Dienes, S. Su, and B. Thomas, Phys. Rev. D **86**, 054008 (2012).

[8] K. R. Dienes, J. Kumar, and B. Thomas, Phys. Rev. D **86**, 055016 (2012).

[9] K. R. Dienes, J. Kumar, and B. Thomas, Phys. Rev. D **88**, 103509 (2013).

[10] I. Cholis and N. Weiner, arXiv:0911.4954.

[11] A. J. Barr, B. Gripaios, and C. G. Lester, J. High Energy Phys. 11 (2009) 096; P. Konar, K. Kong, K. T. Matchev, and M. Park, J. High Energy Phys. 04 (2010) 086.

[12] K. Agashe, D. Kim, M. Toharia, and D. G. E. Walker, Phys. Rev. D **82**, 015007 (2010).
[13] K. Agashe, D. Kim, D. G. E. Walker, and L. Zhu, Phys. Rev. D **84**, 055020 (2011).
[14] K. Agashe, R. Franceschini, D. Kim, and K. Wardlow, Phys. Dark Univ. **2**, 72 (2013).
[15] L. Randall and D. Tucker-Smith, Phys. Rev. Lett. **101**, 221803 (2008).
[16] C. G. Lester and D. J. Summers, Phys. Lett. B **463**, 99 (1999).
[17] A. J. Barr, C. G. Lester, M. A. Parker, B. C. Allanach, and P. Richardson, J. High Energy Phys. 03 (2003) 045; A. Barr, C. Lester, and P. Stephens, J. Phys. G **29**, 2343 (2003).
[18] W. S. Cho, K. Choi, Y. G. Kim, and C. B. Park, Phys. Rev. Lett. **100**, 171801 (2008); J. High Energy Phys. 02 (2008) 035.
[19] M. M. Nojiri, D. Toya, and T. Kobayashi, Phys. Rev. D **62**, 075009 (2000); H.-C. Cheng and J. Gu, J. High Energy Phys. 10 (2011) 094.
[20] D. R. Tovey, J. High Energy Phys. 04 (2008) 034; G. Polesello and D. R. Tovey, J. High Energy Phys. 03 (2010) 030; K. T. Matchev and M. Park, Phys. Rev. Lett. **107**, 061801 (2011).
[21] P. Konar, K. Kong, K. T. Matchev, and M. Park, Phys. Rev. Lett. **105**, 051802 (2010); W. S. Cho, J. E. Kim, and J.-H. Kim, Phys. Rev. D **81**, 095010 (2010); W. S. Cho, W. Klemm, and M. M. Nojiri, Phys. Rev. D **84**, 035018 (2011); C. H. Lally and C. G. Lester, arXiv:1211.1542.
[22] J. Alwall, M. Herquet, F. Maltoni, O. Mattelaer, and T. Stelzer, J. High Energy Phys. 06 (2011) 128.
[23] A. Alloul, N. D. Christensen, C. Degrande, C. Duhr, and B. Fuks, Comput. Phys. Commun. **185**, 2250 (2014).
[24] CMS Collaboration, Report No. CMS-PAS-JME-10-014.
[25] CMS Collaboration, Report No. CMS-PAS-JME-07-003.
[26] S. Chatrchyan *et al.* (CMS Collaboration), Phys. Rev. Lett. **107**, 221804 (2011).
[27] S. Chatrchyan *et al.* (CMS Collaboration), Eur. Phys. J. C **73**, 2568 (2013).
[28] J. Beringer *et al.* (Particle Data Group Collaboration), Phys. Rev. D **86**, 010001 (2012).